J BONE ONCOL 42 (2023) 100502

Contents lists available at ScienceDirect

Journal of Bone Oncology

journal homepage: www.elsevier.com/locate/jbo

Bone tumor examination based on FCNN-4s and CRF fine segmentation fusion algorithm

Shiqiang Wu [a,b,1,*], Xiaoming Bai [b,1], Liquan Cai [a], Liangming Wang [a], XiaoLu Zhang [a], Qingfeng Ke [a], Jianlong Huang [c,d,e,*]

[a] Department of Orthopedics, The Second Affiliated Hospital of Fujian Medical University, Quanzhou, Fujian 362000, China
[b] Department of Orthopedics, The Second Clinical College of Fujian Medical University, Quanzhou, Fujian 362000, China
[c] Faculty of Mathematics and Computer Science, Quanzhou Normal University, Quanzhou 362000, China
[d] Fujian Provincial Key Laboratory of Data Intensive Computing, Quanzhou 362000, China
[e] Key Laboratory of Intelligent Computing and Information Processing, Fujian Province University, Quanzhou 362000, China

HIGHLIGHTS

- Digital image segmentation is crucial for accurate quantitative analysis of medical images, including X-ray images of bone tumors.
- Multi-level feature fusion and batch normalization were used to improve segmentation accuracy in image recognition with a convolutional neural network.
- FCNN-4s algorithm uses fine feature fusion, BN layer, and data augmentation to improve bone tumor segmentation.
- Adopts operations like Crop and Fuse, padding, ReLU activation, and SoftMax loss with optimized hyperparameters for better performance.
- Improves bone tumor segmentation with refined structure and probability graph model, achieving higher accuracy and real-time performance.

ARTICLE INFO

Keywords:
Bone tumor
Image segmentation
Fully convolutional neural network
Conditional random fields
Computed tomography

ABSTRACT

Background and objective: Bone tumor is a kind of harmful orthopedic disease, there are benign and malignant points. Aiming at the problem that the accuracy of the existing machine learning algorithm for bone tumor image segmentation is not high, a bone tumor image segmentation algorithm based on improved full convolutional neural network which consists fully convolutional neural network (FCNN-4s) and conditional random field (CRF).

Methodology: The improved fully convolutional neural network (FCNN-4s) was used to perform coarse segmentation on preprocessed images. Batch normalization layers were added after each convolutional layer to accelerate the convergence speed of network training and improve the accuracy of the trained model. Then, a fully connected conditional random field (CRF) was fused to refine the bone tumor boundary in the coarse segmentation results, achieving the fine segmentation effect.

Results: The experimental results show that compared with the traditional convolutional neural network bone tumor image segmentation algorithm, the algorithm has a great improvement in segmentation accuracy and stability, the average Dice can reach 91.56%, the real-time performance is better.

Conclusion: Compared with the traditional convolutional neural network segmentation algorithm, the algorithm in this paper has a more refined structure, which can effectively solve the problem of over-segmentation and under-segmentation of bone tumors. The segmentation prediction has better real-time performance, strong stability, and can achieve higher segmentation accuracy.

* Corresponding authors at: Department of Orthopedics, The Second Affiliated Hospital of Fujian Medical University, Quanzhou, Fujian 362000, China (S. Wu); Faculty of Mathematics and Computer Science, Quanzhou Normal University, Quanzhou 362000, China (J. Huang).
E-mail addresses: wushiqiang@fjmu.edu.cn (S. Wu), robotics@qztc.edu.cn (J. Huang).
[1] These authors contributed equally to this work.

https://doi.org/10.1016/j.jbo.2023.100502
Received 8 May 2023; Received in revised form 24 August 2023; Accepted 3 September 2023
Available online 6 September 2023

1. Introduction

Bone tumors are a type of orthopedic disease that can be either benign or malignant and pose a significant health risk. The peak incidence of benign bone tumors is between 11 and 20 years of age, while malignant bone tumors tend to occur in individuals aged 20–40 years and often affect long bones, such as the distal femur, proximal tibia, fibular head, distal radius, and proximal humerus [1].

Currently, in clinical diagnosis, only a small portion of the information contained in bone tumor X-rays is typically utilized. Qualitative diagnosis is mainly based on observing the morphological features of the tumor in the X-ray, with little consideration of quantitative parameters such as the shape, texture, and volume of the tumor that are related to the geometry and density information contained in the X-ray. Qualitative diagnosis is subject to the subjectivity of human observers, and different doctors may have inconsistent readings of the same radiograph at different times, which poses significant challenges for clinical diagnosis.

Digital image segmentation is the process of dividing an image into multiple regions based on specific attributes (such as color, texture, density, etc.). Accurate image segmentation is the foundation of quantitative analysis of medical images. Despite the relatively recent emergence of digital image processing, research on image segmentation technology has made considerable progress and success. Zhou et al. [2] proposed a method for recognizing precancerous lesions and cancers in gastric cancer based on the fusion of shallow and deep features in endoscopic images. However, to date, there is still no segmentation method that can be universally applied to all types of images, and not all segmentation methods are suitable for a particular class of images.

Due to the similar X-ray absorption coefficients between tumors and surrounding tissues, as well as the effects of X-ray scattering [3,4], uneven light intensity, and different irradiation angles, the edges of bone tumors in X-ray images appear blurry, and the distribution of tumor and background features overlap. It is necessary to fully consider the local characteristics of the images.

With the rapid development of computer technology, computer vision, image processing, and pattern recognition, digital image segmentation plays an increasingly important role in quantitative analysis of medical images [6]. Among them, MRI and computed tomography (CT) are widely used imaging techniques for detecting abnormalities in tumor shape, size, or location, which help in detecting tumors. Zhao et al. [5] proposed a novel GAN that utilizes its synthesized CT images to visually resemble the reference CT (RCT) images and achieve desirable results on local mismatched tissues. In quantitative evaluation, it outperforms other compared methods. In addition, MRI-guided radiotherapy is a current research hotspot in radiotherapy.

2. Materials and methods

2.1. Basic theory

2.1.1. Improved fully convolutional neural network

In 1998, LeCun et al. [7] first applied CNN to image recognition, and in 2012, the AlexNet network structure proposed by Krizhevsky et al. [8] made significant breakthroughs in the field of CNN object classification. In 2015, Long et al. [9] proposed a pixel-level image semantic segmentation network called Fully Convolutional Neural Network (FCNN), which improved upon AlexNet by performing end-to-end pixel-wise classification and achieving image segmentation tasks. FCNN converted the two fully connected layers of AlexNet into convolutional layers, allowing the network's final output to remain a two-dimensional matrix, thus preserving spatial information between pixels and facilitating feature extraction. To make the output of the network the same size as the input, the original FCNN simply upsampled the output of the last convolutional layer to the same size as the input image, but this operation only utilized information from the 5th pooling layer, resulting in a coarser target feature that made it difficult to achieve precise segmentation.

This algorithm will use feature information from different pooling layers to achieve multi-level feature fusion. After upsampling the output of the last convolutional layer, the first fusion will be performed with the feature vector matrix from the fourth pooling layer, and then the resulting feature fusion matrix will be upsampled and fused with the feature vector matrix from the third pooling layer. Then, the fusion feature matrix will be upsampled and fused with the feature vector matrix from the second pooling layer, and finally, the feature matrix from the third fusion will be upsampled to obtain a feature matrix the same size as the original image, resulting in a better feature information matrix. At the same time, the algorithm adds the batch normalization (BN) layer proposed by Ioffe et al. [10] after each convolutional layer to speed up network training and improve segmentation accuracy. The network structure with multi-level feature fusion is shown in Fig. 1, where Conv represents a convolutional layer that can extract various features of the image such as edges and positions, Pool represents a pooling layer that can achieve feature dimensionality reduction and preserve the main features extracted by the convolutional layer, BN represents a batch normalization layer that ensures that the weight distribution of the network after convolution does not change significantly, Up represents an upsampling layer that mainly increases the size of the feature matrix through deconvolution, Crop_Fuse performs cropping and fusion operations on the feature matrix, and Pixelwise Prediction is the pixel-wise classification prediction layer that achieves image segmentation by classifying each pixel.

2.1.2. Conditional random field

Conditional Random Field (CRF) based image semantic segmentation is one of the classic probabilistic graphical segmentation algorithms, which can remove noise in the segmentation result and enhance the boundary segmentation of the image. This algorithm integrates the fully connected CRF model proposed by Zheng et al. [11] into the improved FCNN network for post-processing bone tumor boundary segmentation, thereby improving the segmentation accuracy of bone tumor images.

In the fully connected CRF model, the energy function that assigns pixels to their respective labels can be represented as:

$$E(x) = \sum_{i} \varphi_u(x_i) + \sum_{i \neq j} \varphi_p(x_i, x_j) \tag{1}$$

In Equation (1), $E(x)$ represents the total energy of assigning pixels to their respective labels; $\varphi_u(x_i)$ is a unary energy potential function that represents the energy of assigning pixel i to label x_i without considering the relationship between pixels; $\varphi_p(x_i, x_j)$ is a pairwise energy potential function that represents the energy of assigning pixels i and j to labels x_i and x_j based on the difference in grayscale values and spatial position distances between pixels, and describes the relationships between pairwise pixels, such that similar pixels are assigned the same label. The unary energy potential function $\varphi_u(x_i)$ can be obtained from the initial coarse segmentation result of FCNN, and the pairwise energy potential function $\varphi_p(x_i, x_j)$ can be represented as:

$$\varphi_p(x_i, x_j) = \mu(x_i, x_j) \sum_{m=1}^{M} W^{(m)} k_G^{(m)}(f_i, f_j) \tag{2}$$

In Equation (2), $\mu(x_i, x_j)$ is the label compatibility matrix, which represents the penalty for assigning different labels to different pixels. When $x_i \neq x_j$, the penalty $\mu(x_i, x_j) = 1$; $k_G^{(m)}(f_i, f_j)$ is the Gaussian filter kernel, where f_i, and f_j are the feature vectors of the filter, determined by the spatial position between pixels and their grayscale values, and m is the number of filters; $W^{(m)}$ is the weight of each filter.

In the CRF model, a bilateral Gaussian filter is used to assign pixels that are close in space and have similar grayscale values to the same label; a spatially smooth Gaussian filter is used to remove isolated small

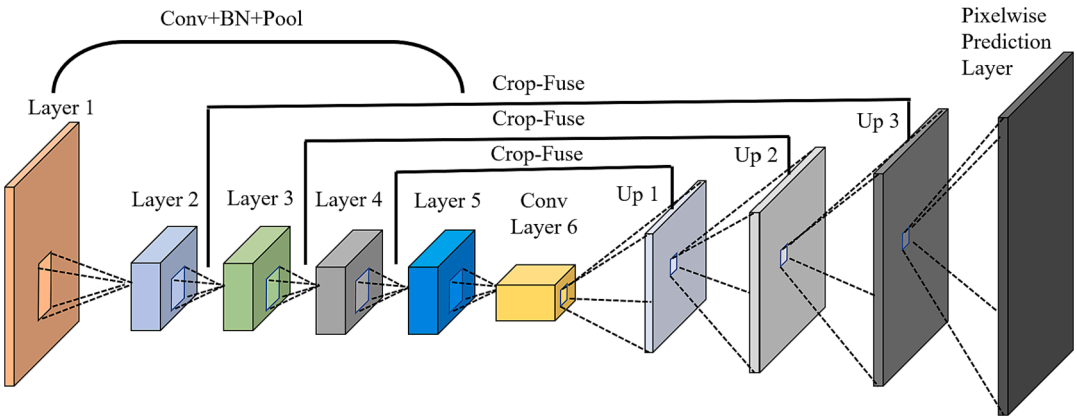

Fig. 1. The network structure chart of the multilevel features information fusion.

regions in the bone tumor segmentation result. Therefore, Equation (2) can be further represented as:

$$\varphi_p(x_i, x_j) = \mu(x_i, x_j)\left[W^{(1)}\exp\left(-\frac{|P_i - P_j|}{2\theta_\alpha^2} - \frac{|R_i - R_j|}{2\theta_\beta^2}\right) + W^{(2)}\exp\left(-\frac{|P_i - P_j|}{2\theta_\gamma^2}\right)\right] \quad (3)$$

In Equation (3), R_i and R_j represent the grayscale feature value vectors of pixels i and j; P_i and P_j represent the spatial position relationship feature vectors of pixels i and j; θ_α、θ_β and θ_γ represent the weights of the grayscale, position, and other factors on the potential functions of the pixels. Zheng et al. [9] have conducted a large number of experiments and found that when the bilateral filter weight $W^{(1)} = 5$, the control parameters $\theta_\alpha = 160$、$\theta_\beta = 3$, the smoothing filter weight $W^{(2)} = 3$, and the control parameter $\theta_\gamma = 5$, the boundary of the image can be better segmented.

2.2. Algorithms used in this paper

In this paper, the algorithm flow of bone tumor image segmentation using the improved full convolutional neural network is shown in Fig. 2. Firstly, the collected images are preprocessed. Then, part of the processed data is used as the training set and the rest as the test set. This training set is used to train FCNN and CRF fusion algorithm. Finally, the model is tested on the test set, and the segmentation results are evaluated using performance indicators. Figs. 3–5.

2.2.1. Image preprocessing

Each pixel in the original CT bone tumor image is stored in the computer as 16 bits, but in digital image processing, 8-bit images are commonly used. Therefore, in this study, the CT images were first normalized in terms of gray level, with the gray values of each pixel uniformly compressed to the range of 0–255.

2.2.2. Improved FCNN-4s coarse segmentation algorithm

In order to obtain good tumor features, this paper proposes a fine feature fusion model and adds a BN layer to the network. The FCNN-4s algorithm includes a data layer, convolution layer, pooling layer, activation function layer, upsampling layer, and output probability map layer. The feature fusion operation (Fuse) is used to fuse the features of high-dimensional feature matrices and low-dimensional feature matrices, and the data of the corresponding dimensions of the two matrices are added together under the premise of the same dimension and size. If the dimensions and sizes of the two target matrices are not the same, the FCNN-4s algorithm will perform a matrix cropping operation (Crop) to make their dimensions and sizes the same, so that the

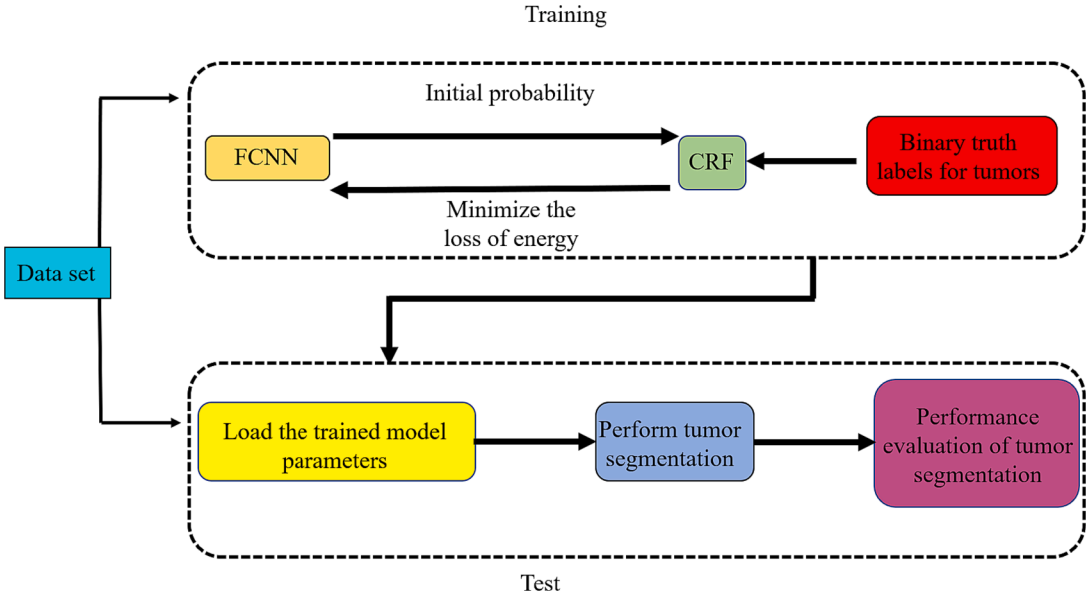

Fig. 2. The flow chart of algorithm.

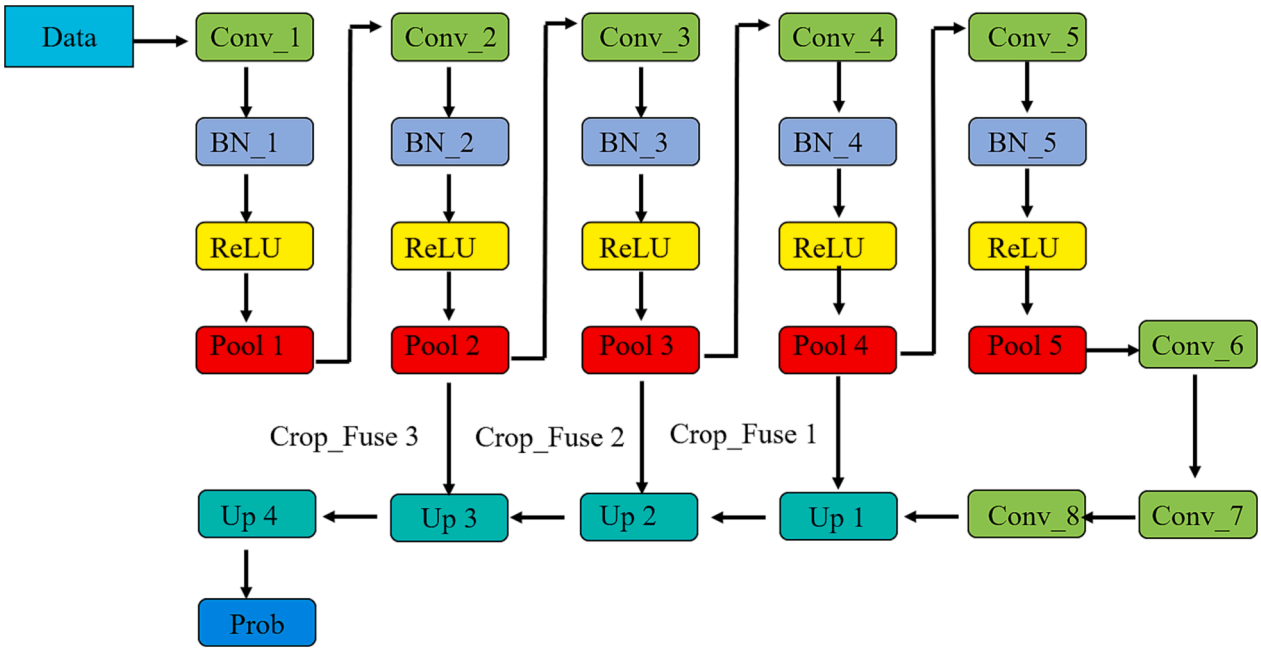

Fig. 3. The network structure chart of the improved FCNN-4s.

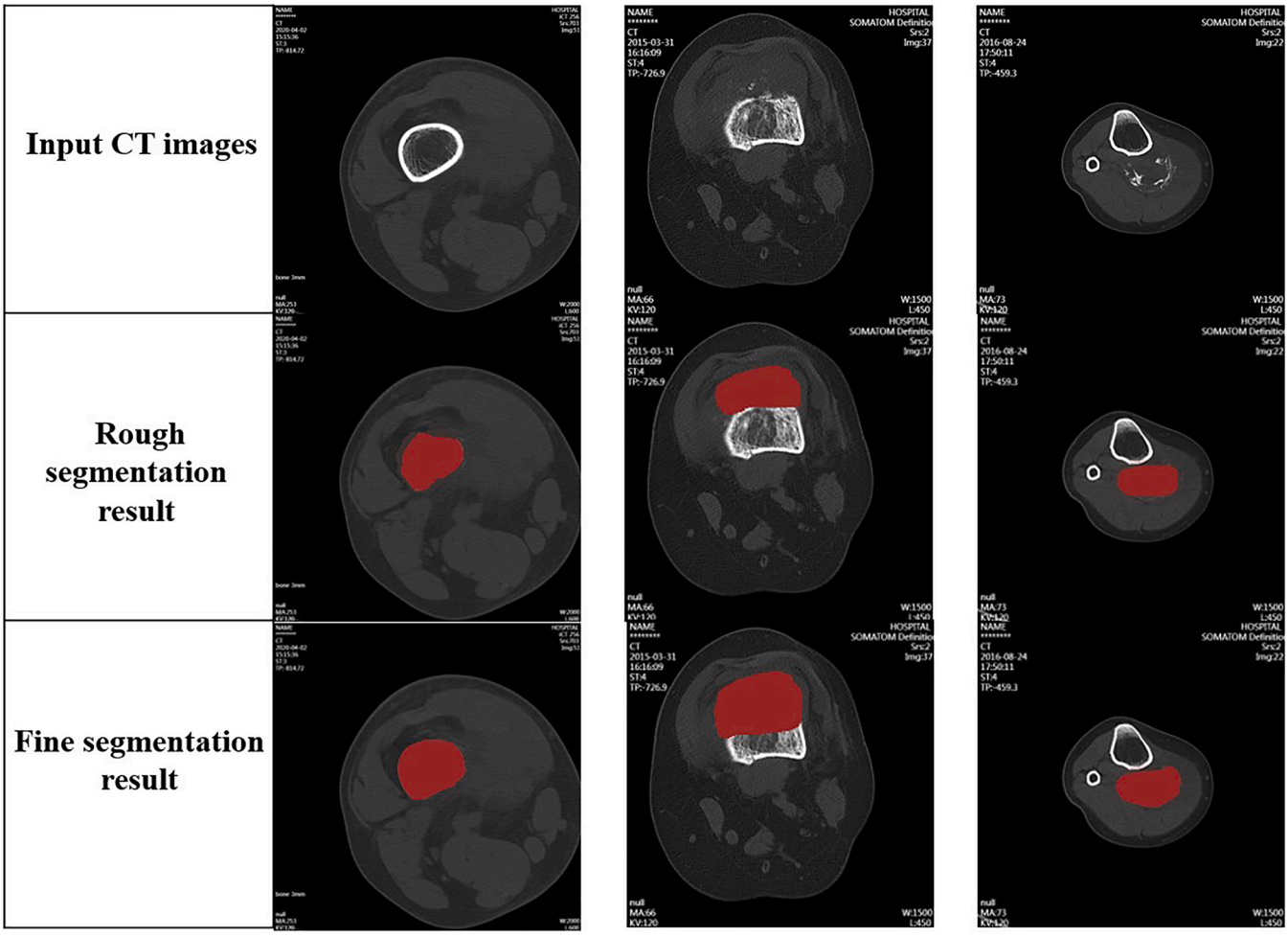

Fig. 4. The results of coarse segmentation and fine segmentation are compared.

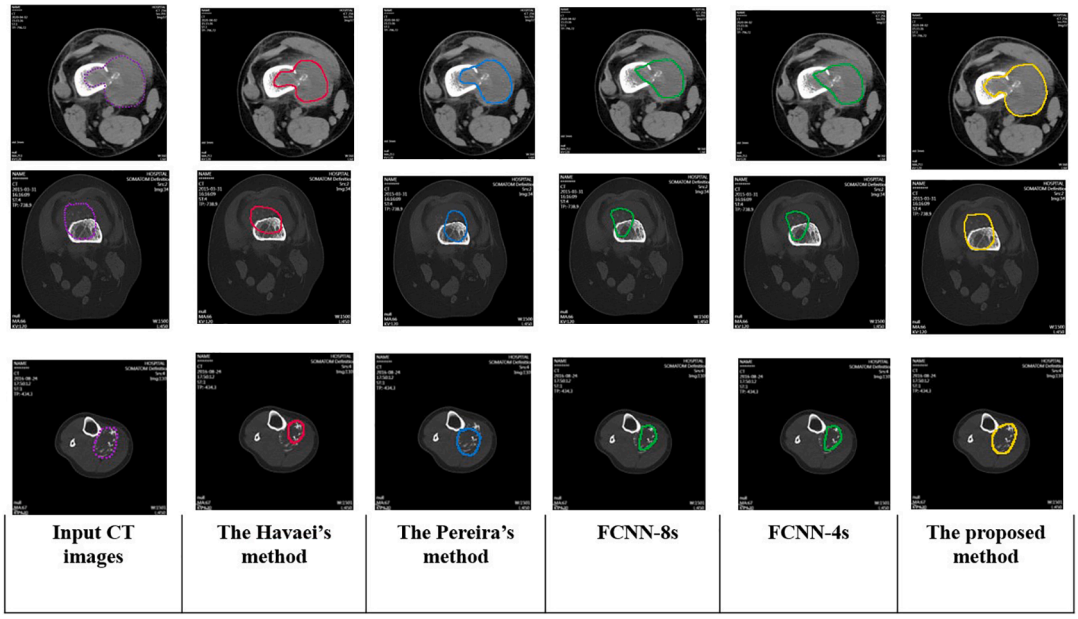

Fig. 5. Compared with the segmentation results of five segmentation methods.

network can smoothly learn the features. In the matrix cropping operation, if the dimensions are different, the low-dimensional feature matrix is convolved to make the two matrices have the same dimensions; if the sizes are different, the same size as the high-dimensional feature matrix is extracted symmetrically from the center of the low-dimensional feature matrix. These operations are all designed to improve the performance of the network and achieve better bone tumor segmentation results. To prevent the feature information matrix from becoming too small after pooling, this paper performs a padding operation on the original bone tumor image (240×240) with a padding size of 100. The output size indicates the dimension and size of the output feature matrix. The algorithm performs three fusion operations on the feature matrices of different dimensions to obtain more refined bone tumor features. Meanwhile, the BN layer can keep the weight distribution of the parameters during each iteration from changing significantly, thereby accelerating the convergence speed.

2.2.3. Fine segmentation fusion algorithm of FCNN-4s and CRF

This paper describes the process of determining whether each pixel in an CT bone tumor image is a tumor point, using a binary classification approach where the label "0″ represents non-tumor pixels and "1″ represents tumor pixels. After obtaining two initial probability maps from FCNN-4s, the energy function is initialized to obtain the original probability values for each pixel. The following steps are used to calculate the CRF model and iteratively adjust the two-class probability maps predicted by FCNN-4s using a fusion algorithm.

Step 1: Involving filtering the probability maps for both classes using a Gaussian filter $k_G^{(m)}\left(f_i, f_j\right)$ to obtain two filtered results $\widetilde{Q}^{(m)}(l)$ for labels "0″ and "1″, respectively.

Step 2: Assigning weights $W^{(m)}$ to $\widetilde{Q}^{(m)}(l)$ and calculates the pairwise energy potential function $\varphi_p(x_i, l)$ for each class probability map based on the label compatibility matrix $\mu^{(m)}(x_i, l)$.

Step 3: Calculating the unary energy potential function $\varphi_u(x_i)$ for the output of the FCNN-4s network, and then integrates it with the pairwise energy potential function $\varphi_p(x_i, l)$ from Step 2 to obtain the overall energy function $\widehat{Q}_i(x_i)$.

Step 4: Normalizing $\widehat{Q}_i(x_i)$ to obtain the probability values for each pixel's label,denoted as $Q_i(x_i)$. and selects the label with the highest probability for each pixel. The algorithm loop continues until the probability values for each pixel's label converge to 90% or more, at which point the algorithm stops. If the convergence threshold is not met, the pixel loss is back-propagated to the FCNN-4s algorithm for further learning and parameter adjustment.

The pseudo-code for the algorithm is shown below, which results in a fusion network structure of CRF and FCNN-4s. The end-to-end calculation of the loss and parameter updates for each pixel can be performed using the back-propagation algorithm.

Begin

$Q_i(x_i) \leftarrow \frac{1}{Z_i}\exp(-\varphi_u(x_i))$ for all x_i, Z is the normalization factor.

While not converged $Q_i(x_i) \geqslant 90\%$ do

$\widetilde{Q}_i^{(m)}(l) \leftarrow \sum_{j \neq i} k_G^{(m)}\left(f_i, f_j\right) Q_j(l)$ for $m = 2$;

$\varphi_p(x_i, l) \leftarrow \sum_{l \in L} \mu^{(m)}(x_i, l) \sum_{m=1}^{2} W^{(m)} \widetilde{Q}_i^{(m)}(l)$;

$\widehat{Q}_i(x_i) \leftarrow \varphi_u(x_i) + \varphi_p(x_i, l)$;

$Q_i(x_i) \leftarrow \frac{1}{Z}\exp(-\widehat{Q}_i(x_i))$;

end while

End

2.3. Data set and image preprocessing

The images used in the experiments were collected from the Second Affiliated Hospital of Fujian Medical University. The three-dimensional size of each CT image is 240×240×155, and the ground truth labels are manually annotated by five experts.

In this experiment, 150 CT images of bone tumors were randomly selected as the training set. The image preprocessing techniques and data augmentation techniques described in section 2.2.1 were used to obtain a total of 48,000 training images with a size of 240×240. This paper mainly performed data augmentation on the bone tumor images, including horizontal and vertical flipping, as well as counterclockwise rotation by 90°, 180°, and 270°, to improve the accuracy of the trained model.

3. Results

3.1. Evaluation criteria

This paper evaluates the segmentation results of bone tumors using indicators such as the Dice Similarity Coefficient (DSC), sensitivity, and positive predictive value (PPV). The DSC represents the similarity be-

tween the experimental segmentation results and the labels, sensitivity represents the ratio of correctly segmented tumor points to the true tumor points, and PPV represents the ratio of correctly segmented tumor points to the total segmented tumor points. The formulas are as follows:

$$\text{Dice} = \frac{|P \wedge T|}{(|P| + |T|)/2} \tag{4}$$

$$\text{Sensitivity} = \frac{|P \wedge T|}{|T|} \tag{5}$$

$$\text{Positive} = \frac{|P \wedge T|}{|P|} \tag{6}$$

In the formulas, P represents the segmentation results obtained using the algorithm proposed in this paper, while T represents the labels generated by experts for the bone tumors.

3.2. Model training process

During the training stage, the mature Caffe deep learning framework was used to learn the model parameters on the training set. Considering that Sigmoid and Tanh activation functions easily cause gradient disappearance, ReLU was chosen as the activation function for the network, and the conventional SoftMax classification loss function was used.

Since the selection of learning rate is crucial to the network and determines whether the network can converge and to what degree, it cannot be too large or too small. In this paper, the convergence of the network under different learning rates was compared using the original training set. According to the experimental results, when the network selects relatively large learning rates such as 10e-08 and 10e-09, the training loss cannot converge. When the learning rate is 10e-10, the training loss can converge and the convergence is better than that of smaller learning rates such as 10e-11. Therefore, a learning rate of 10e-10 was ultimately adopted.

The weight decay coefficient has a certain impact on the degree of overfitting of the network. This paper compared the training accuracy of the network under different weight decay coefficients. The experimental results showed that when the weight decay coefficient is too small, it has not played a role in weight decay and the training accuracy of the network is poor. When the weight decay coefficient is too large, the network will be overfitting to some extent and the training accuracy will decrease. Therefore, a weight decay coefficient of 0.0005 was ultimately adopted.

To verify the effectiveness of adding BN layers, this paper compared the training loss and accuracy of the network before and after adding BN layers using the original training set. The network with BN layers had a loss of about 5000 after 8000 iterations, and the network had basically converged after $1.2x10^5$ iterations. In contrast, the network without BN layers had a loss of about 5000 after $2.0x10^4$ iterations, and the network converged after nearly $1.6x10^5$ iterations, which fully demonstrates that BN layers can speed up the convergence of the network and reduce the loss value. Adding BN layers also improves the accuracy of the trained model to some extent.

After selecting the network structure and parameters correctly, to verify the influence of augmented datasets on the model accuracy, this paper compared the tumor classification accuracy on different datasets. As the dataset was gradually augmented, the training accuracy improved significantly. This indicates that increasing training samples can prevent network overfitting and improve the model's generalization ability, which ensures that the trained model can achieve good bone tumor segmentation on the test set.

3.3. Comparison of segmentation results between single-mode image and fused mode image

This paper proposes a bone tumor segmentation model that combines coarse segmentation and fine segmentation to improve segmentation accuracy. F. 7 shows the results of our algorithm for coarse and fine segmentation, where the red contour represents the position of the bone tumor. It can be seen that our algorithm is able to accurately locate and segment the bone tumor, and precisely outline the contour of the tumor with a small error compared to the ground truth.

Subsequently, three metrics were used to quantitatively analyze the segmentation results, as shown in Table 1. It can be seen that the fine segmentation model has significantly improved segmentation accuracy in terms of metrics such as the similarity index, sensitivity, and positive predictive value, compared to the coarse segmentation model. In particular, the positive predictive value has increased by 6.15%.

4. Discussion

In order to verify the superiority of the proposed improved algorithm, this paper compared it with the simple segmentation algorithm FCNN-8s, which only performs two feature fusions, and FCNN-4s algorithm without CRF fusion. The experiment also compared with traditional CNN algorithms proposed by famous scholars Havaei [12] and Pereira [13]. From F. 8, it can be seen that the Havaei [12] algorithm has obvious over-segmentation, the segmentation of bone tumor boundaries is not clear and there are many isolated scatter points. The Pereira [13] algorithm has better segmentation accuracy due to its deeper network, and its performance is slightly better than the Huawei algorithm, which also reduces the over-segmentation of bone tumors to a certain extent. Although FCNN-8s obtained a smooth bone tumor segmentation contour, the feature fusion is relatively less, which resulted in insufficiently fine bone tumor boundaries and low segmentation accuracy. Compared to FCNN-8s, FCNN-4s has some enhancement in obtaining bone tumor boundary information, but the segmented bone tumor boundary is still not delicate enough. Especially in the segmentation of the third complex bone tumor image, the segmentation results of various algorithms are unsatisfactory due to the complexity of the tumor boundary. However, the proposed algorithm can still obtain satisfactory results. Overall, the FCNN-4s model with more fine feature fusion and the end-to-end algorithm structure formed by fusing CRF can make similar pixels obtain the same label, refine the bone tumor boundary, and effectively solve the problems of over-segmentation and under-segmentation of bone tumors.

Additionally, as shown in Table 2, the proposed algorithm has higher segmentation accuracy compared to other algorithms. The Dice coefficient is improved by 6.78% and 3.95% compared to the algorithms proposed by two other scholars, respectively, and on average, it is improved by 9.16% compared to the FCNN algorithm without fusion CRF. Moreover, in terms of the average time for segmenting a bone tumor image, the proposed algorithm has high real-time performance in the prediction stage, with an average time of 1 s to complete the segmentation of a bone tumor image.

Other types of deep learning algorithms such as U-Net [17,18,19] may also be implemented for tumor segmentation. U-Net is a popular deep learning algorithm that has shown promising results in various medical image segmentation tasks, including tumor segmentation. It is a type of convolutional neural network that is designed to learn from both

Table 1
Segmentation performance evaluation of different segmentation algorithms.

Different segmentation algorithm	Dice	Sensitivity	Positive
Improved FCNN-4s rough segmentation algorithm	0.8746	0.8692	0.8561
Fine segmentation fusion algorithm of FCNN-4s and CRF	0.9122	0.9215	0.9176

Table 2
The segmentation performance evaluation of five algorithms.

Different segmentation algorithm	Dice	Sensitivity	Positive	The average time to complete an image segmentation
Havaei	0.8478	0.8127	0.8344	2.8842
Pereira	0.8761	0.8854	0.8852	3.5468
FCNN-4s	0.8467	0.8672	0.8674	0.9735
FCNN-8s	0.8013	0.8425	0.8617	0.8946
The algorithm proposed in this paper	0.9156	0.8976	0.9008	1.0547

low-level and high-level features of the image, allowing for more accurate and robust segmentation. U-Net has been used in several studies for tumor segmentation, and its performance has been shown to be comparable or even superior to other segmentation methods. Its ability to handle complex and irregular shapes of tumors makes it a suitable choice for many medical image analysis applications.

Cancer spread and controllable treatment can also be analysed visually discrete element method [4]. and also by state-of-the-art graphical and meshing algorithms [1516]. These type of computer simulations is able to assist and improve bone cancer diagnosis, which is advances orthopedics diagnosis. Note that the use of deep learning is vital in this aspects of computer aided diagnostics and will be a promising technology [20,21].

5. . Conclusion

This paper proposes an improved bone tumor image segmentation algorithm to address the shortcomings of traditional convolutional neural network (CNN) algorithms, such as high computational complexity and low accuracy. The proposed algorithm uses an improved fully convolutional neural network to achieve coarse segmentation of bone tumor pixels and a probability graph model that fuses the correlation between image labels, and the conditional random field is used to form a trainable end-to-end segmentation algorithm. Compared with traditional CNN segmentation algorithms, the structure of this algorithm is more refined, which can effectively solve the problem of over-segmentation and under-segmentation of bone tumors, and has better segmentation prediction real-time performance and stability, achieving higher segmentation accuracy. The experimental results show that the proposed algorithm has higher segmentation accuracy than other algorithms and has high real-time performance in the average time required for segmentation of a bone tumor image, with an average of 1 s to complete the segmentation of a bone tumor image.

Declaration of Competing Interest

The authors declare that they have no known competing financial interests or personal relationships that could have appeared to influence the work reported in this paper.

Acknowledgment

This research is supported by Natural Science Foundation Project of Fujian Province (No.2021J01274)

References

[1] Y.P. Lu, et al., Practical Orthopedics, People's Military Medical Press, Beijing, 1991.
[2] H. Zhou, Z. Liu, T. Li, Y. Chen, W. Huang, Z. Zhang, Classification of precancerous lesions based on fusion of multiple hierarchical features, Computer methods and programs in biomedicine 229 (2023) 107301.
[3] P.K. Sahoo, S. Soltani, A.K.C. Wong, A survey of thresholding techniques, Computer Vision and Graphics Image Processing. 41 (3) (1988) 233–260.
[4] N.R. Pal, S.K. Pal, A review of image segmentation techniques, Pattern Recognition. 26 (9) (1993) 1277–1294.
[5] B.o. Zhao, T. Cheng, X. Zhang, J. Wang, H. Zhu, R. Zhao, D. Li, Z. Zhang, G. Yu, CT synthesis from MR in the pelvic area using Residual Transformer Conditional GAN, Computerized medical imaging and graphics 103 (2023) 102150.
[6] S. Lu, Z. Zhang, Z. Yan, Y. Wang, T. Cheng, R. Zhou, G. Yang, Mutually aided uncertainty incorporated Dual Consistency Regularization with Pseudo Label for Semi-Supervised Medical Image Segmentation, Neurocomputing 126411 (2023).
[7] Y. Lecun, L. Bottou, Y. Bengio, P. Haffner, Gradient-based learning applied to document recognition, Proceedings of the IEEE. 86 (11) (1998) 2278–2324.
[8] Krizhevsky A, Sutskever I, Hinton GE. ImageNet classification with deep convolutional neural networks. In: International Conference on Neural Information Processing Systems. Curran Associates Inc. 2012. 1097-1105.
[9] J. Long, E. Shelhamer, T. Darrell, Fully convolutional networks for semantic segmentation, In: Computer Vision and Pattern Recognition. IEEE (2015) 3431–3440.
[10] S. Ioffe, C. Szegedy, Batch normalization,, accelerating deep network training by reducing internal covariate shift, In: International Conference on Machine Learning. JMLR.org (2015) 448–456.
[11] S. Zheng, S. Jayasumana, B. Romera-Paredes, et al., Conditional Random Fields as Recurrent Neural Networks, in: In: IEEE International Conference on Computer Vision, IEEE, 2016, pp. 1529–1537.
[12] M. Havaei, A. Davy, D. Warde-Farley, A. Biard, A. Courville, Y. Bengio, C. Pal, P.-M. Jodoin, H. Larochelle, Brain tumor segmentation with Deep Neural Networks, Medical Image Analysis. 35 (2017) 18–31.
[13] S. Pereira, A. Pinto, V. Alves, C.A. Silva, Brain Tumor Segmentation Using Convolutional Neural Networks in MRI Images, IEEE Transactions on Medical Imaging. 35 (5) (2016) 1240–1251.
[15] M. Wei, Q. Wang, Y. Li, W.-M. Pang, L. Liang, J. Wang, K.K.L. Wong, D. Abbott, J. Qin, J. Wu, Centerline Extraction of Vasculature Mesh, IEEE Access (2017), https://doi.org/10.1109/ACCESS.2018.2802478.
[16] C. Zhao, C.F. Lui, S. Du, D.i. Wang, Y. Shao, Fai Chun lul, Shichang Du, Di Wang, and Yiping Shao, An Earth Mover's Distance based Multivariate Generalized Likelihood Ratio Control Chart for Effective Monitoring of 3D Point Cloud Surface, Computers & Industrial Engineering 175 (2023) 108911.
[17] M. Zhao, Y. Wei, Y.u. Lu, K.K.L. Wong, A novel U-Net approach to segment the cardiac chamber in magnetic resonance images with ghost artifacts, Computer Methods and Programs in Biomedicine 196 (2020) 105623.
[18] X. Zhu, Y. Wei, Y.u. Lu, M. Zhao, K.e. Yang, S. Wu, H. Zhang, K.K.L. Wong, Comparative analysis of active contour and convolutional neural network in rapid left-ventricle volume quantification using echocardiographic imaging, Computer Methods and Programs in Biomedicine 199 (2021) 105914.
[19] K.K.L. Wong, A.n. Zhang, K.e. Yang, S. Wu, D.N. Ghista, GCW-UNet segmentation of cardiac magnetic resonance images for evaluation of left atrial enlargement, Computer Methods and Programs in Biomedicine 221 (2022) 106915.
[20] K.K.L. Wong, G. Fortino, D. Abbott, Deep learning-based cardiovascular image diagnosis: A promising challenge, Future Generation Computer Systems 110 (2020) 802–811.
[21] K.K.L. Wong, Z. Sun, J.Y. Tu, S.G. Worthley, J. Mazumdar, D. Abbott, Medical image diagnostics based on computer-aided flow analysis using magnetic resonance images, Computerized Medical Imaging and Graphics 36 (7) (2012) 527–541.

Further reading

[14] K.K.L. Wong, Three-dimensional discrete element method for the prediction of protoplasmic seepage through membrane in a biological cell, Journal of Biomechanics 8 (65) (2017) 115–124.